

---

# 3D Gaussian Splatting as Markov Chain Monte Carlo

---

Shakiba Kheradmand<sup>1</sup>, Daniel Rebain<sup>1</sup>, Gopal Sharma<sup>1</sup>,  
Weiwei Sun<sup>1</sup>, Jeff Tseng<sup>1</sup>, Hossam Isack<sup>2</sup>,  
Abhishek Kar<sup>2</sup>, Andrea Tagliasacchi<sup>3,4,5</sup>, Kwang Moo Yi<sup>1</sup>

<sup>1</sup> University of British Columbia, <sup>2</sup> Google Research,  
<sup>3</sup> Google DeepMind, <sup>4</sup> Simon Fraser University, <sup>5</sup> University of Toronto

## Abstract

While 3D Gaussian Splatting has recently become popular for neural rendering, current methods rely on carefully engineered cloning and splitting strategies for placing Gaussians, which does not always generalize and may lead to poor-quality renderings. In addition, for real-world scenes, they rely on a good initial point cloud to perform well. In this work, we rethink 3D Gaussians as random samples drawn from an underlying probability distribution describing the physical representation of the scene—in other words, Markov Chain Monte Carlo (MCMC) samples. Under this view, we show that the 3D Gaussian updates are strikingly similar to a Stochastic Langevin Gradient Descent (SGLD) update. As with MCMC, samples are nothing but past visit locations, adding new Gaussians under our framework can simply be realized without heuristics as placing Gaussians at existing Gaussian locations. To encourage using fewer Gaussians for efficiency, we introduce an L1-regularizer on the Gaussians. On various standard evaluation scenes, we show that our method provides improved rendering quality, easy control over the number of Gaussians, and robustness to initialization.

## 1 Introduction

Neural rendering has seen a significant advancement with the introduction of Neural Radiance Fields (NeRF) [16], and more recently, 3D Gaussian Splatting (3DGS) [9]. 3D Gaussian Splatting became highly popular thanks to its speed and efficiency—it can render high-quality images in a fraction of the time required by NeRF. Unsurprisingly, various extensions to 3D Gaussian Splatting have been proposed, such as extending 3D Gaussians to dynamic scenes [24, 22], making them robust to aliasing effects [27, 23], and applications into generative 3D content creation [31, 28, 19] to name a few.

However, despite the various extensions, a common shortcoming of these methods is that they mostly rely on the same initialization and densification strategy for placing the Gaussians—the one originally suggested by [9]. Specifically, they rely on carefully engineered cloning and splitting strategies for placing Gaussians, called adaptive density control, one that is purely heuristic. Depending on the state of each Gaussian, they are cloned, split, or pruned, which is how the number of Gaussians is controlled. Moreover, Gaussians are regularly ‘reset’ by setting their opacities to small values. This heuristic-based approach requires multiple hyperparameters to be carefully tuned and as we will show later, can fail in new scenes.

Besides the engineered heuristics, there are a few limitations with the original 3DGS approach. Most importantly, a good initial point cloud is required for real-world scenes in order to achieve the highest outcome. Furthermore, it is not straightforward to estimate how many 3D Gaussians will be used

for a given scene from just the hyperparameters—making it difficult to control the computation and memory budget in advance without affecting reconstruction quality during inference-time. Moreover, these heuristics do not always generalize well, and in some cases, lead to suboptimal placement of Gaussians, resulting in poor-quality renderings and wasted compute.

To solve this problem, we take a step back and rethink 3D Gaussians as a sample-based representation of scenes—as Markov Chain Monte Carlo (MCMC) samples. We view 3D Gaussians as random samples that are drawn from an underlying probability distribution that models the 3D scene. In fact, under this view, we show in Section 3.2 that the conventional 3D Gaussian Splatting update rule is similar to a Stochastic Gradient Langevin Dynamics update [3, 10]. It only lacks the noise term that promotes the exploration of samples. We thus reformulate 3D Gaussian Splatting into an SGLD framework, an MCMC algorithm, which naturally explores the scene landscape and would provide Gaussians sampled at locations that are closely tied with the likelihood of the scene. It is important to note that while we assume an underlying distribution, this distribution does not need to be explicitly modeled, with Gaussians as MCMC, the Gaussians themselves are already representing it.

Given this view, the heuristics involved in placing and identifying Gaussians, as well as resetting their opacities, are no longer necessary. 3D Gaussians are simply the samples used for MCMC, thus exploring their sample locations are naturally dealt with through the SGLD updates. Adding Gaussians is now simply increasing the number of samples, which in the case of the MCMC, is equivalent to observing more of the recently visited locations. In other words, we add Gaussians by simply selecting a randomly chosen Gaussian based on the opacity values as an indicator of high probability regions, and adding a small new Gaussian at its location. When doing so, this simple strategy, under the MCMC framework, is enough to provide renderings of high quality, beyond what is provided by the conventional heuristics. Also, to improve the convergence speed, we resample Gaussians when they are invisible to where the probability is high.

Finally, to encourage that we use the least number of Gaussians possible, we apply L1-regularization to encourage sparsity. We apply regularization to both the opacity and the scale of Gaussians, effectively encouraging them to ‘disappear’ if unnecessary.

We evaluate our method on standard scenes evaluated in [9] (NeRF Synthetic [16], MipNeRF 360 [2], Tank & Temples [12], and Deep Blending [8]). With our method, one does not need to carefully initialize the Gaussians — Our method provides high-quality renderings, regardless of whether Gaussians are initialized randomly or from Structure-from-Motion points.

To summarize, our contributions are:

- we rethink Gaussians in Gaussian Splatting as samples from a distribution that represents the 3D scene, which allows simplification;
- we improve robustness to initialization.
- we propose to simply add samples and resample by drawing samples from existing Gaussian locations under the SGLD paradigm;
- we introduce L1 regularization on opacity and scale to encourage using fewer Gaussians and increase efficiency and performance;
- we provide higher rendering quality when the heuristics are a limiting factor;

## 2 Related Work

We first briefly review recent advances in novel-view synthesis via neural rendering, and discuss more recent works related to 3D Gaussian Splatting [9].

**Novel-view synthesis via Neural Radiance Fields.** Since the introduction of Neural Radiance Fields (NeRF) [16], it has become extremely popular for building and representing 3D scenes. The core idea behind the method is to learn a Neural Field that encodes radiance values in the modeling volume, which is then used to render via volume rendering with light rays. Since its first introduction, it has been extended to deal with few views [26], to generalize to new scenes without training [18, 26], to dynamic scenes [6], to unbound scenes [2], to unposed or roughly posed images [21], to speed up training [17, 25], and even to those that focus on biomedical applications [5, 30] to name a few. These extensions are by no means an exhaustive list and demonstrate the impact that NeRF had. For a more in-depth survey we refer the readers to [7].

Amongst works on NeRF, most relevant to ours is [10], which also employs Stochastic Gradient Langevin Dynamics (SGLD) [3], in their case to identify the most promising samples to train with and allow faster convergence of Neural Field training. While we ground ourselves in the same Markov Chain Monte Carlo (MCMC) paradigm based on SGLD, the application context is entirely different. In their work, SGLD is used to perform a form of soft mining rays to accelerate the training of NeRF. In our case, we are instead rethinking Gaussian Splatting as samples from an underlying distribution that better represents the 3D scene.

**Gaussian Splatting.** 3D Gaussian Splatting [9] is a recent alternative to NeRF that rely on differentiable rasterization instead of volume rendering. In a nutshell, instead of quering points along the ray, it stores Gaussians, which can then be rasterized into each view to form images. This rasterization operation is highly efficient, as now, instead of querying hundreds of points along a light ray to render a pixel, one can simply rasterize the few Gaussians associated to the pixel. Therefore, Gaussian Splatting allows 1080p images to be rendered at 130 frames per second on modern GPUs, which sparked interest from the research community.

Unsurprisingly, various extensions immediately followed. These include ones that focus on removing aliasing effects [27, 23], on dynamic scenes [22, 24], on 3D content generation [19, 31, 28], and on controllable 3D avatars [13]. All of these extensions are extremely recent, demonstrating the large interest. One core limitation that these methods share though, is that they all rely on the original heuristics that 3D Gaussian Splatting [9] suggested when it comes to densifying and pruning Gaussians. As we demonstrate in this work, this does not necessarily always work, and require either careful initialization and tuning. Even then, the rendering outcomes may be suboptimal. We further direct interested readers to a very recent survey on Gaussian Splatting-based methods [4].

### 3 Method

We first reformulate Gaussian Splatting as Markov Chain Monte Carlo (MCMC) sampling. We then introduce the new update equations under the MCMC framework with Stochastic Gradient Langevin Dynamics [3, 10]. We then discuss the specifics of how we add new Gaussians, the L1 regularization to encourage fewer Gaussians to be used, and the implementation details.

#### 3.1 Brief review of 3D Gaussian Splatting

Before reformulating, we first briefly review 3D Gaussian Splatting [9] for completeness. 3D Gaussian Splatting represents the scene as a set of 3D Gaussians, which are then rasterized into a desired view via point-based  $\alpha$ -blending. This can be viewed as an efficient way to perform volume rendering as in NeRFs [16]. Specifically, for a camera pose  $\theta$  to render a pixel  $\mathbf{x}$  we order the  $N$  Gaussians by sorting them in the order of increasing distance from the camera and write

$$\mathbf{C}(\mathbf{x}) = \sum_{i=1}^N \mathbf{c}_i \alpha_i(\mathbf{x}) \left[ \prod_{j=1}^{i-1} (1 - \alpha_j(\mathbf{x})) \right], \quad (1)$$

where  $\mathbf{c}_i$  is the color of each Gaussian and if we denote their opacity as  $o$ , centers as  $\boldsymbol{\mu}$ , and covariance as  $\boldsymbol{\Sigma}$ , we write

$$\alpha_i(\mathbf{x}) = o_i \exp\left(-\frac{1}{2}(\mathbf{x} - \mathcal{J}_\theta(\boldsymbol{\mu}_i))^T \mathcal{J}_\theta(\boldsymbol{\Sigma}_i)^{-1}(\mathbf{x} - \mathcal{J}_\theta(\boldsymbol{\mu}_i))\right), \quad (2)$$

where  $\mathcal{J}$  is the camera projection. Then, with the color values for each pixel, Gaussians are trained to minimize the loss

$$\mathcal{L}_{\text{total}} = (1 - \lambda_{\text{D-SSIM}})\mathcal{L}_1 + \lambda_{\text{D-SSIM}}\mathcal{L}_{\text{D-SSIM}}, \quad (3)$$

where  $\mathcal{L}_1$  is the average L1 error between  $\mathbf{C}(\mathbf{x})$  and the ground-truth colour  $\mathbf{C}_{\text{gt}}(\mathbf{x})$ , and  $\mathcal{L}_{\text{D-SSIM}}$  is the Structural Similarity Index Metric (SSIM) [20] between the rendered and ground-truth image. We follow [9] and use  $\lambda_{\text{D-SSIM}}=0.2$ .

It is worth noticing that the entire process, at a high level, can be abstracted as an operation on top of a set of Gaussians that turn them into colors. In other words, dropping the notations for pixel coordinate  $\mathbf{x}$  and summarizing each Gaussian as  $\mathbf{g}_i$  for simplicity, we write

$$\mathbf{C} = \mathcal{R}_\theta(\{\mathbf{g}_i\}_{i=1\dots N}), \quad (4)$$

where  $\mathcal{R}_\theta$  denotes the entire view-dependant rendering process. We now use this simplified notation to introduce our idea of viewing 3D Gaussian Splatting as MCMC.

### 3.2 3D Gaussian Splatting as Markov Chain Monte Carlo (MCMC)

We note that with Eq. (4), one can think of a situation where  $N \rightarrow \infty$ , which in that case the set of Gaussians  $\{\mathbf{g}_i\}_{i=1\dots N}$  will become a distribution. Conversely, denoting this distribution as  $\mathcal{G}$ , we can rewrite Eq. (4) as

$$\mathbf{C} = \mathcal{R}_\theta(\{\mathbf{g}_1, \mathbf{g}_2, \dots, \mathbf{g}_N \mid \mathbf{g}_i \sim \mathcal{G}\}). \quad (5)$$

It is important to notice that in Eq. (4), one does *not* have to explicitly model  $\mathcal{G}$ , but instead can opt for an MCMC strategy, where one only needs to evaluate where samples should move to next to properly represent  $\mathcal{G}$ . Interestingly, moving Gaussians to better locations is what standard 3D Gaussian Splatting already does, although purely based on gradients, and with heuristics governing whether each sample is cloned, split, pruned, or even reset.

Upon a closer look, the way 3D Gaussian Splatting updates Gaussians closely resembles a Stochastic Gradient Langevin Dynamics (SGLD) [3] update scheme, which has also been very recently explored for Neural Fields [10]. Specifically, in the case of standard 3D Gaussian Splatting,  $\mathbf{g}_i$ , with the exception of heuristics, are updated via their gradients, that is

$$\mathbf{g}_i \leftarrow \mathbf{g}_i - \lambda_{\text{lr}} \nabla_{\mathbf{g}_i} \mathcal{L}_{\text{total}}, \quad (6)$$

where  $\lambda_{\text{lr}}$  is the learning rate. An SGLD update, on the other hand, would be in the form of

$$\mathbf{g}_i \leftarrow \mathbf{g}_i + a \nabla_{\mathbf{g}_i} \log \mathcal{P} + b \epsilon, \quad (7)$$

where  $a$  and  $b$  are hyperparameters controlling the convergence speed and exploration parameters,<sup>1</sup> respectively,  $\mathcal{P}$  is the distribution one wishes to sample from, and  $\epsilon$  is the noise distribution for exploration. We note the striking similarity between Eq. (6) and Eq. (7). In other words, having the loss as the negative log likelihood of the underlying distribution, that is,

$$\mathcal{G} = \mathcal{P} \propto \exp(-\mathcal{L}_{\text{total}}), \quad (8)$$

both equations are identical up to hyperparameter level, and up to the absence of the noise distribution in Eq. (6). Hence, the standard Gaussian Splatting could be understood as having Gaussians that are sampled from a likelihood distribution that is tied to the rendering quality, once the noise is introduced.

### 3.3 Updating with Adam Stochastic Gradient Langevin Dynamics

With the connection between SGLD and already existing 3D Gaussian Splatting updates, we now rewrite the update equation as

$$\mathbf{g}_i \leftarrow \mathbf{g}_i - \lambda_{\text{lr}} \nabla_{\mathbf{g}_i} \mathcal{L}_{\text{total}} + \lambda_{\text{noise}} \epsilon_i, \quad (9)$$

where  $\lambda_{\text{lr}}$  and  $\lambda_{\text{beta}}$  are the hyperparameters controlling the learning rate and the amount of exploration enforced by SGLD. In practice, instead of the raw gradients  $\nabla_{\mathbf{g}_i} \mathcal{L}_{\text{total}}$ , we use the Adam [11] optimizer with default parameters for  $\beta_1$  and  $\beta_2$  [14].

In Eq. (9), it is important that the noise term  $\epsilon_i$  is designed carefully. The noise term  $\epsilon_i$  needs to be added in a way that it can be ‘mitigated’ by the gradient term  $\nabla_{\mathbf{g}_i} \mathcal{L}_{\text{total}}$  if necessary, or otherwise the Eq. (9) reduces to a pure noise-based update. For example, certain Gaussians on a smooth region can have wide support, while others in highly textured regions can be narrow. For narrow regions, adding a noise that goes beyond the support of the Gaussian would be irrecoverable, which should be avoided. Learning rate should also be considered in this regard. Additionally, considering that the noise term essentially translates to exploration, we notice that Gaussians well-behave when they are properly located, and most of where exploration is needed is their spatial location. In other words, exploration is not critical for opacity, scale, and color, and we do not add noise. We thus design the noise term *only on the center locations of the Gaussians* such that it is dependent on their covariances and also its opacities, as well as the learning rate. We write

$$\epsilon_i = \lambda_{\text{lr}} \Sigma_i \sigma(-k(o_i - t)) \eta, \quad (10)$$

<sup>1</sup>These two hyperparameters are interconnected, but we denote them separately for simplicity in notation following [10].



where  $\eta \sim \mathcal{N}(\mathbf{0}, \mathbf{I})$ ,  $\sigma$  is the sigmoid function, and  $k$  and  $t$  are hyperparameters controlling the sharpness of the sigmoid, which we set as  $k=100$  and  $t=(1 - 0.005)$  to make a sharp transition function that goes from zero to one, centered around the default pruning threshold of 3D Gaussian Splatting [9] for the opacity values of Gaussians.

### 3.4 Encouraging fewer Gaussians

To make effective use of the memory and computation, and to improve the performance, we encourage fewer Gaussians to be used via regularization. Instead of a heuristic pruning strategy, we simply encourage sparsity via regularization.

As the existence of a Gaussian is effectively determined by its opacity  $o$  and covariance  $\Sigma$ , we apply regularization to both of these. We thus write

$$\mathcal{L}_{\text{total}} = (1 - \lambda_{\text{D-SSIM}})\mathcal{L}_1 + \lambda_{\text{D-SSIM}}\mathcal{L}_{\text{D-SSIM}} + \lambda_o\mathbb{E}_i|o_i|_1 + \lambda_{\Sigma}\mathbb{E}_i|\sqrt{\text{eig}(\Sigma_i)}|_1, \quad (11)$$

where  $\text{eig}(\cdot)$  denotes the eigenvalues of the covariance matrix (the standard deviations along the principle axes of the covariance matrix), and  $\lambda_o$  and  $\lambda_{\Sigma}$  are hyperparameters controlling the regularization strength. Note that the additional regularizers will encourage opacity and covariance to be small, at which point, effectively makes them disappear. Furthermore, Gaussians with small scale leads to faster inference as each Gaussian is drawn on fewer pixels.

### 3.5 Implementation Details

**Adding Gaussians** In the MCMC framework, sample locations represent the positions visited by samples as they move through the sampling space. Therefore, incorporating a new Gaussian entails choosing one of the previous paths, meaning one of the current Gaussians. Thus, we add the new small Gaussians with a default opacity value to an existing Gaussian location. We select these locations based on the opacity of Gaussians, i.e. more likelihood for a Gaussian with large opacity, thus encouraging new samples to lie in regions of higher density. Additionally, we limit the number of newly added Gaussians during training to 5% of the entire number of Gaussians to prevent newly added Gaussians from significantly disturbing the MCMC sampling process. We found this simple strategy to be highly effective, as we show later in Section 4.

**Teleporting Gaussians** Throughout the training, some Gaussians will die with small enough opacity to not contribute to the renderings, which in turn leads to solely noise-based update. Every 100 iterations, we opt to teleport [15] Gaussians with opacity below a threshold to high opacity region as explained above. Specifically, we consider Gaussians with opacity smaller than 0.005 as dead, following the default pruning threshold of 3D Gaussian Splatting [9]. However, instead of simply pruning as in the conventional heuristic, we opt to move the sample’s degree of freedom to another sample. Specifically, we clone an existing Gaussian with everything the same but lower opacity values. We also reset the optimizer’s state of the original Gaussians.

**Initialization and training.** We initialize our samples either randomly or from point clouds, typically either from Structure-from-Motion (SfM) or LiDAR as in 3D Gaussian Splatting [9]. For random initialization, we follow their strategy and uniformly random sample  $100k$  Gaussians within three times the extent of the camera bounding box. We also follow the same learning rate and learning-rate scheduling as well. For position, we start at learning rate of  $1.6e^{-4}$  and decay it exponentially to  $1.6e^{-6}$ .

Afterward, we gradually increase the number of Gaussians to the desired pre-defined number of Gaussians. Specifically, similar to how 3D Gaussian Splatting [9] does its heuristics every 100 iterations, we also add points and resample every 100 iterations. As discussed in Section 3.5, we make sure to not add more than 5% of the total number of Gaussians, to not disrupt the MCMC sampling process.

Table 1: **Quantitative results with same number of Gaussians** – We report results using PSNR, SSIM and LPIPS metrics. Our method significantly outperforms all baselines even when starting from random initialization, with a large gap in performance when compared with 3DGS [9]–random.

	NeRF Synthetic [16]	MipNeRF 360 [2]	Tank & Temples [12]	Deep Blending [8]
	PSNR↑ / SSIM↑ / LPIPS↓	PSNR↑ / SSIM↑ / LPIPS↓	PSNR↑ / SSIM↑ / LPIPS↓	PSNR↑ / SSIM↑ / LPIPS↓
NeRF [17]	31.01 / - / -	24.85 / 0.66 / 0.43	-	21.18 / 0.78 / 0.34
Plenoxels [25]	31.76 / - / -	23.63 / 0.67 / 0.44	21.08 / 0.72 / 0.38	-
INGP-Big [17]	33.18 / - / -	26.75 / 0.75 / 0.30	21.92 / 0.75 / 0.31	-
MipNeRF [1]	33.09 / - / -	27.60 / 0.81 / 0.25	-	21.54 / 0.78 / 0.37
MipNeRF360 [2]	-	29.23 / 0.84 / 0.21	22.22 / 0.76 / 0.26	-
3DGS [9]—paper	33.32 / - / -	28.69 / 0.87 / 0.18	23.14 / 0.84 / 0.18	-
3DGS [9]-Random.	33.42 / 0.97 / 0.04	27.89 / 0.84 / 0.26	21.93 / 0.79 / 0.27	29.55 / 0.90 / 0.33
Ours-Random.	<b>33.85 / 0.97 / 0.04</b>	<b>29.58 / 0.89 / 0.19</b>	<b>24.47 / 0.86 / 0.19</b>	<b>29.66 / 0.90 / 0.31</b>
3DGS [9]	-	29.30 / 0.88 / 0.21	23.67 / 0.84 / 0.22	29.64 / 0.90 / 0.32
Ours	-	<b>29.83 / 0.89 / 0.19</b>	<b>24.19 / 0.86 / 0.18</b>	<b>29.80 / 0.90 / 0.30</b>

## 4 Experiments

### 4.1 Dataset and experimental setup

**Datasets.** We use various datasets, both synthetic and real, following [9]. Specifically, for the scenes used by [9], we use all scenes from NeRF Synthetic [16] dataset, two scenes from the Tank & Temples [12], two scenes from the Deep Blending [8] and all publicly available scenes from MipNeRF 360 [2]. In the main paper, we report our results by summarizing the average statistics for each dataset.

**Metrics.** We evaluate each method using three standard metrics: Peak Signal-to-Noise Ratio (PSNR), Structural Similarity Index Metric (SSIM) [20], and Learned Perceptual Image Patch Similarity (LPIPS) [29].

**Baselines.** We compare against conventional 3D Gaussian Splatting (3DGS) [9], with both random and point cloud-based initialization strategies—we denote the latter with the ‘random’ suffix. We also include state-of-the-art baselines for each dataset as a reference.

### 4.2 Results

We perform our experiments with the same number of Gaussians being used as the standard heuristics to demonstrate how our method performs under a similar Gaussian budget. Table 1 and Fig. 1 provide quantitative and qualitative visualization of our results and compare it with the baseline in the Figure. To be on fair ground, we simply look at the maximum number of Gaussians that the conventional method converges to, and choose this value as the as the maximum limit on number of Gaussains for our method.

When using the same number of Gaussians, our method provides better performance to 3D Gaussian Splatting [9] when Gaussians are initialized with point clouds, which already is a carefully tuned scenario. Of particular interest is again when points are randomly initialized, where our method significantly outperforms original 3D Gaussian Splatting [9] which starts from SFM point clouds. This results demonstrates the effectiveness of the MCMC formulation over heuristics.

### 4.3 Ablation studies

We further evaluate whether our regularizer can help conventional 3D Gaussian Splatting as well. As shown in Table 2, this is not the case. This is to be expected, given that the hyperparameters for the conventional heuristics are tightly coupled with how the loss behaves. Hence, introducing these regularizers would require another round of careful hyperparameter tuning.

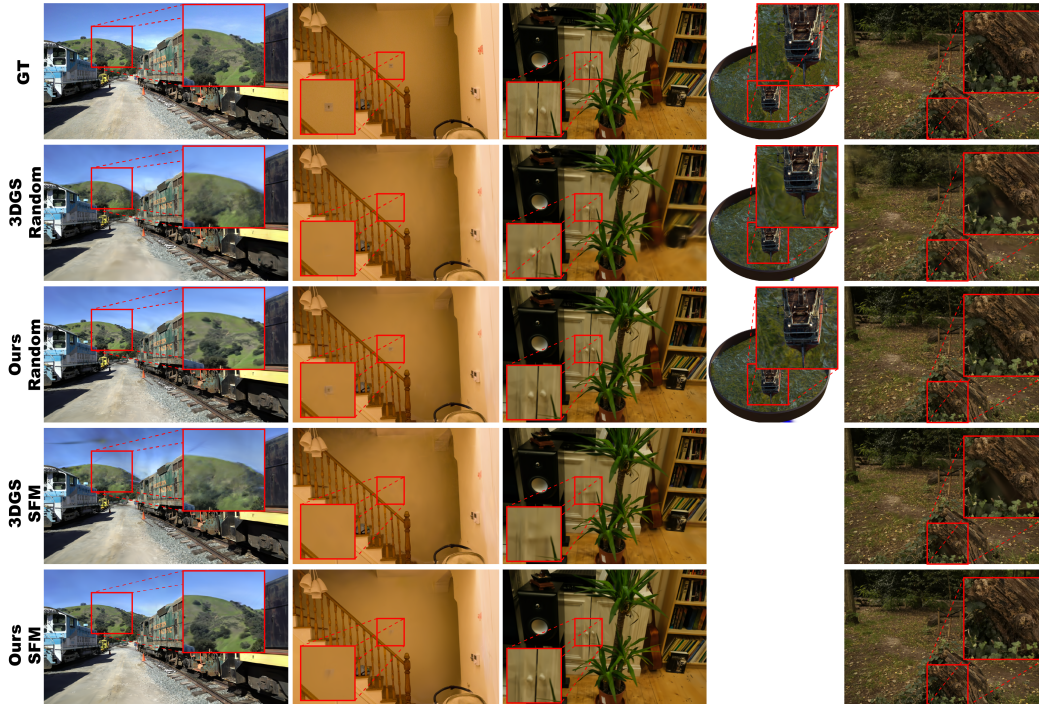


Figure 1: **Qualitative highlights with the same number of Gaussians** – We provide examples of novel-view rendering of 3DGS [9] and our approach with random or SFM based initialization on multiple scenes from different datasets. We highlight the differences in inset figures. Our method faithfully represents details of the various regions thanks to our MCMC-based re-formulation that places Gaussians in a principled manner, with theoretical guarantees of MCMC providing support. Our results provide higher PSNR overall as well. Please zoom-in to see details.



Figure 2: **Effect of the noise term ( $\epsilon$ )**– We visualize our reconstruction that uses noise term (Eq. 9) in the left half of each rendering and without the noise in the right half. The noise added to the gradients during sampling encourages exploration which allows better reconstruction.

Furthermore, Table 2 provides the effect of regularization and noise term in our results. As can be seen, both components are essential for the best performance. Fig. 2 shows the effect of noise on the generated outcome. As you can see, noise term help the exploration.

Table 2: **Ablation study** – We report the PSNR, SSIM, and LPIPS metrics with varying components of our method removed, as well as the L1 regularizer being added to 3D Gaussian Splatting [9], all starting from random initialization. All components contribute to the final rendering quality.

	3DGS [9]	3DGS [9] + L1 reg.	Ours w/o L1 reg.	Ours w/o Noise	Ours w L1 reg. & Noise
counter	28.09 / 0.88 / 0.30	25.03 / 0.87 / 0.30	17.60 / 0.63 / 0.62	27.07 / 0.87 / 0.30	<b>29.20 / 0.92 / 0.23</b>
stump	23.91 / 0.68 / 0.33	19.65 / 0.50 / 0.53	19.47 / 0.36 / 0.69	20.89 / 0.51 / 0.45	<b>27.49 / 0.81 / 0.20</b>
kitchen	30.54 / 0.92 / 0.16	25.89 / 0.90 / 0.20	21.05 / 0.56 / 0.59	28.97 / 0.89 / 0.21	<b>31.62 / 0.93 / 0.14</b>
bicycle	24.57 / 0.70 / 0.33	20.48 / 0.62 / 0.40	17.37 / 0.33 / 0.71	23.19 / 0.67 / 0.33	<b>25.91 / 0.81 / 0.19</b>
bonsai	30.94 / 0.93 / 0.26	25.27 / 0.86 / 0.34	19.03 / 0.64 / 0.60	29.92 / 0.91 / 0.30	<b>32.55 / 0.95 / 0.23</b>
room	30.04 / 0.90 / 0.32	27.93 / 0.89 / 0.32	19.44 / 0.71 / 0.59	28.74 / 0.89 / 0.33	<b>32.51 / 0.94 / 0.25</b>
garden	27.16 / 0.86 / 0.14	22.60 / 0.73 / 0.25	19.91 / 0.39 / 0.63	26.17 / 0.82 / 0.18	<b>27.78 / 0.88 / 0.12</b>
Avg.	27.89 / 0.84 / 0.26	23.84 / 0.77 / 0.33	19.12 / 0.52 / 0.63	26.42 / 0.79 / 0.30	<b>29.58 / 0.89 / 0.19</b>

## 5 Conclusion

In this paper, we have reformulated 3D Gaussian Splatting [9] as Markov Chain Monte Carlo (MCMC) that is implemented via Adam Stochastic Langevin Gradient Dynamics (SGLD). By doing so, we show that we can eliminate the need for a good initial estimate, and avoid heuristic-based densification, pruning and reset. We show that this strategy generalizes well across all scenes originally used to test 3D Gaussian Splatting [9].

## References

- [1] Barron, J.T., Mildenhall, B., Tancik, M., Hedman, P., Martin-Brualla, R., Srinivasan, P.P.: Mip-nerf: A multiscale representation for anti-aliasing neural radiance fields. In: Proceedings of the IEEE/CVF International Conference on Computer Vision. pp. 5855–5864 (2021)
- [2] Barron, J.T., Mildenhall, B., Verbin, D., Srinivasan, P.P., Hedman, P.: Mip-nerf 360: Unbounded anti-aliased neural radiance fields. In: Proceedings of the IEEE/CVF Conference on Computer Vision and Pattern Recognition. pp. 5470–5479 (2022)
- [3] Brosse, N., Moulines, E., Durmus, A.: The Promises and Pitfalls of Stochastic Gradient Langevin Dynamics. In: Adv. Neural Inform. Process. Syst. (2018)
- [4] Chen, G., Wang, W.: A survey on 3d gaussian splatting. arXiv preprint arXiv:2401.03890 (2024)
- [5] Corona-Figueroa, A., Frawley, J., Bond-Taylor, S., Bethapudi, S., Shum, H.P.H., Willcocks, C.G.: Mednerf: Medical neural radiance fields for reconstructing 3d-aware ct-projections from a single x-ray (2022)
- [6] Gafni, G., Thies, J., Zollhofer, M., Niessner, M.: Dynamic neural radiance fields for monocular 4D facial avatar reconstruction. <https://arxiv.org/abs/2012.03065> (2020)
- [7] Gao, K., Gao, Y., He, H., Lu, D., Xu, L., Li, J.: Nerf: Neural radiance field in 3d vision, a comprehensive review. arXiv preprint arXiv:2210.00379 (2022)
- [8] Hedman, P., Philip, J., Price, T., Frahm, J.M., Drettakis, G., Brostow, G.: Deep blending for free-viewpoint image-based rendering. *ACM Transactions on Graphics (ToG)* **37**(6), 1–15 (2018)
- [9] Kerbl, B., Kopanas, G., Leimkuhler, T., Drettakis, G.: 3d gaussian splatting for real-time radiance field rendering. *ACM Transactions on Graphics* **42**(4) (2023)
- [10] Kheradmand, S., Rebain, D., Sharma, G., Isack, H., Kar, A., Tagliasacchi, A., Yi, K.M.: Accelerating Neural Field Training via Soft Mining. In: IEEE Conf. Comput. Vis. Pattern Recog. (2024)
- [11] Kingma, D.P., Ba, J.: Adam: A method for stochastic optimisation. In: Int. Conf. Learn. Represent. (2015)

- [12] Knapitsch, A., Park, J., Zhou, Q.Y., Koltun, V.: Tanks and temples: Benchmarking large-scale scene reconstruction. *ACM Transactions on Graphics (ToG)* **36**(4), 1–13 (2017)
- [13] Kocabas, M., Chang, J.H.R., Gabriel, J., Tuzel, O., Ranjan, A.: Hugs: Human gaussian splats. *arXiv preprint arXiv:2311.17910* (2023)
- [14] Li, J., Wang, W., Ji, H.: Self-supervised deep learning for image reconstruction: A langevin monte carlo approach. *SIAM Journal on Imaging Sciences* **16**(4), 2247–2284 (2023)
- [15] Lindsey, M., Weare, J., Zhang, A.: Ensemble markov chain monte carlo with teleporting walkers. *SIAM/ASA Journal on Uncertainty Quantification* **10**(3), 860–885 (2022)
- [16] Mildenhall, B., Srinivasan, P.P., Tancik, M., Barron, J.T., Ramamoorthi, R., Ng, R.: Nerf: Representing scenes as neural radiance fields for view synthesis. *Communications of the ACM* **65**(1), 99–106 (2021)
- [17] Muller, T., Evans, A., Schied, C., Keller, A.: Instant neural graphics primitives with a multiresolution hash encoding. *ACM Trans. Graph.* **41**(4), 102:1–102:15 (Jul 2022)
- [18] Rematas, K., Brualla, R.M., Ferrari, V.: ShaRF: Shape-conditioned radiance fields from a single view. <https://arxiv.org/pdf/2102.08860.pdf> (2021)
- [19] Tang, J., Ren, J., Zhou, H., Liu, Z., Zeng, G.: Dreamgaussian: Generative gaussian splatting for efficient 3d content creation. *arXiv preprint arXiv:2309.16653* (2023)
- [20] Wang, Z., Bovik, A.C., Sheikh, H.R., Simoncelli, E.P.: Image quality assessment: From error visibility to structural similarity. *IEEE Trans. Image Process.* **13**(4), 600–612 (2004)
- [21] Wang, Z., Wu, S., Xie, W., Chen, M., Prisacariu, V.A.: NeRF-: Neural radiance fields without known camera parameters. <https://arxiv.org/abs/2102.07064> (2021)
- [22] Wu, G., Yi, T., Fang, J., Xie, L., Zhang, X., Wei, W., Liu, W., Tian, Q., Wang, X.: 4d gaussian splatting for real-time dynamic scene rendering. *arXiv preprint arXiv:2310.08528* (2023)
- [23] Yan, Z., Low, W.F., Chen, Y., Lee, G.H.: Multi-scale 3d gaussian splatting for anti-aliased rendering. *arXiv preprint arXiv:2311.17089* (2023)
- [24] Yang, Z., Gao, X., Zhou, W., Jiao, S., Zhang, Y., Jin, X.: Deformable 3d gaussians for high-fidelity monocular dynamic scene reconstruction. *arXiv preprint arXiv:2309.13101* (2023)
- [25] Yu, A., Li, R., Tancik, M., Li, H., Ng, R., Kanazawa, A.: Plenotrees for real-time rendering of neural radiance fields. In: *arXiv* (2021)
- [26] Yu, A., Ye, V., Tancik, M., Kanazawa, A.: pixelnerf: Neural radiance fields from one or few images. In: *IEEE Conf. Comput. Vis. Pattern Recog.* pp. 4578–4587 (2021)
- [27] Yu, Z., Chen, A., Huang, B., Sattler, T., Geiger, A.: Mip-splatting: Alias-free 3d gaussian splatting. *arXiv preprint arXiv:2311.16493* (2023)
- [28] Yuan, Y., Li, X., Huang, Y., De Mello, S., Nagano, K., Kautz, J., Iqbal, U.: Gavatar: Animatable 3d gaussian avatars with implicit mesh learning. *arXiv preprint arXiv:2312.11461* (2023)
- [29] Zhang, R., Isola, P., Efros, A.A., Shechtman, E., Wang, O.: The Unreasonable Effectiveness of Deep Features as a Perceptual Metric. In: *IEEE Conf. Comput. Vis. Pattern Recog.* (2018)
- [30] Zhong, E.D., Lerer, A., Davis, J.H., Berger, B.: Cryodrgn2: Ab initio neural reconstruction of 3d protein structures from real cryo-em images. In: *Int. Conf. Comput. Vis.* pp. 4046–4055 (2021). <https://doi.org/10.1109/ICCV48922.2021.00403>
- [31] Zou, Z.X., Yu, Z., Guo, Y.C., Li, Y., Liang, D., Cao, Y.P., Zhang, S.H.: Triplane meets gaussian splatting: Fast and generalizable single-view 3d reconstruction with transformers. *arXiv preprint arXiv:2312.09147* (2023)